RESEARCH PAPER

Exploring the Role of Nanosphere Plasmonic Structures on the Efficiency Enhancement of Copper Indium Gallium Diselenide Solar Cells

Marzieh Akbari[1], Fatemeh Dabbagh Kashani[1,*], Seyed Mohammad Mirkazemi[2]

* f_dk@iust.ac.ir

[1] School of Physics, Iran University of Science and Technology, Tehran, Iran
[2] School of Metallurgy and Materials Engineering, Iran University of Science and Technology, Tehran, Iran

Abstract: CIGS solar cells are currently very high-efficiency thin-film solar cells. Concerning higher efficiency in solar cells, research is being conducted on the influence of both light scattering and plasmonic resonances due to metallic nano-structures. This article discusses the assessment of the incorporation of plasmonic nanostructures on the absorber layer of a 1000 nm CIGS solar cell, in terms of light absorption and device performance. It is noted that decisions on material, size, and surface coverage (Occupied Factor) were essential considerations that affected the performance. Opto-electrical assessment was used to investigate absorption, charge-carrier generation, current density-voltage response, power-voltage properties, and total efficiency. Using simulations, we discovered the aluminum nanosphere arrays (200 nm diameter, Occupied Factor 0.64) at the top of the absorber layer yielded the maximum efficiency (26.14%). The resonances showed this, and the near-field distribution garnered from the nanospheres boosts charge carrier generation, diminishes recombination losses, and increases charge separation. Collectively, these raised the performance of the CIGS solar cells in this research and suggested hope for moving CIGS and potentially other photovoltaics forward using nanoscale plasmonic resonances.

Keywords: Chalcopyrite solar cell, Finite-Difference Time-Domain (FDTD) technique, Noble metals, Plasmonic resonances, Characterizations of optical and electrical properties.

1. INTRODUCTION

Solar energy depends on the construction of reasonably priced and effective conversion methods. Since the 1980s, CIGS solar cells have become one of the most viable options for solar applications due to their high efficiency, low cost, customizable direct bandgap, and high light absorption [1-5]. Newer advances in research and development of CIGS solar cells have driven them to commerciality over the past several years. The late 2000s were pivotal due to several breakthroughs, as research brought CIGS solar cell efficiency above 20%, and eventually to over 23% efficiency, vastly outpacing traditional silicon solar cells, which can reach a maximum efficiency of around 21.25% [6-12]. Although CIGS solar cells have exceeded 23% efficiency, these cells are also below the Shockley-Queisser limit, and they can still improve [13, 14]. To enhance the efficiency of CIGS, the following strategies may be employed: altering the materials and thicknesses of the layers, bandgap tuning, doping, and selenizing or annealing. Other methods include adding hole transport or reflective layers, improving surface morphology, optimising light management, utilising mesh and window layers,

and making better back contacts [15-21]. Nevertheless, to further improve performance and achieve the full benefits of CIGS solar cells, researchers are working on next-level light-trapping strategies and plasmonic nanostructures [22-31]. Plasmonic nanostructures may hold great promise to enhance the optical and electrical properties of CIGS solar cells and facilitate the formation of next-generation high-efficiency photovoltaics. However, CIGS solar cells still suffer with respect to absorber thickness, thereby limiting optimal light absorption and confinement [32, 33]. Researchers are currently investigating integrating plasmonic nanostructures to reduce light trapping problems and improve the efficiency of CIGS solar cells. These nanostructures exploit the unique optical characteristics of noble metal nanoparticles to control light–matter interactions. Plasmonic nanostructures can be used to help mitigate the barriers to CIGS architectures with the design and integration of the strategy [24-28]. Plasmonic nanostructures offer many advantages that can help enhance the efficiencies of CIGS solar cells. With respect to light absorption and scattering, plasmonic nanostructures improve the optical path in the absorber layer by allowing increased interaction with incident photons and

1

CIGS material. The localized surface plasmon resonance (LSPR) effect creates a greater electric field around the nanoparticles, improving the chances of generating electron–hole pairs, ultimately lowering recombination losses and increasing photocurrent and overall efficiency. [14, 24-29]. More effective light absorption will allow for thinner CIGS layers, which reduces costs and allows for light and flexible solar cells. Plasmonic structures can absorb light over a broader range than some wavelength-specific methods, which only absorb a particular color. The nanoplasmonic particles can be integrated into CIGS in a manufacturing-friendly way, therefore maintaining engineering and commercialization capacity. In addition, cheap materials, which aluminum generally is, can give the best combination [22, 24-29].

This study evaluates the performance of silver, gold, and aluminium nano spheres on solar cell performance, examining the varying effects of spherical size, occupied factors, and nanosphere positions. The paper describes the device structure and simulation methods, including a comparison of the cell models with and without nanoplasmonic features. The simulations examine how the arrangement of plasmonic nanoparticle arrays can impact the opto-electrical properties, light absorption, and efficiency of CIGS. Through plasmonic methods, the CIGS layer thickness can effectively be cut to 1000 nm, demonstrating a lower cost for materials. The conclusions provide references for optimizing solar cells and improving efficiency for energy conversion.

2. EXPERIMENTAL PROCEDURES

The divergence of the Poynting vector is commonly used when quantifying absorption (and can be numerically sensitive). A modified version of the equation with improved stability allows accurate assessment of absorption characteristics [34, 35].

$$P_{abs} = -0.5\omega|E|^2 imag(\varepsilon) \tag{1}$$

To identify the absorption, only the intensity of the electric field (E) and the imaginary component of the permittivity (ε) are needed; ω is the frequency. With these parameters, it is simple to measure the absorption in an FDTD simulation. The purpose of this calculation is to determine the number of photons absorbed per unit volume, assuming that each absorbed photon in the active layer generates an exciton. To find the number of absorbed photons per volume, we divide the absorbed power (P_{abs})

by the energy of each of the photons, where $\hbar$ is the Planck constant [36].

$$g = P_{abs}/\hbar\omega = -0.5|E|^2 imag(\varepsilon)/\hbar \tag{2}$$

The efficiency (η) represents its capability to transform sunlight into electricity and is calculated as follows [37]:

$$\eta = FF \times V_\infty \times J_{SC}/S_{AM1.5G} \tag{3}$$

Where FF is the fill factor, V_{oc} is the open-circuit voltage, J_{sc} is the short-circuit current density, and the incident power from the AM1.5G solar model, which is set at 100 mW/cm² and referred to as $S_{AM1.5G}$. During absorption computation, key considerations include layer arrangement, material types, computation space, boundary conditions, mesh size, and solving Maxwell's equations using the FDTD method within the unit cell (Yee cell) (Fig. 1). The simulation uses cubic unit cells in a Cartesian grid, aligning E-field and H-field components accordingly [38].
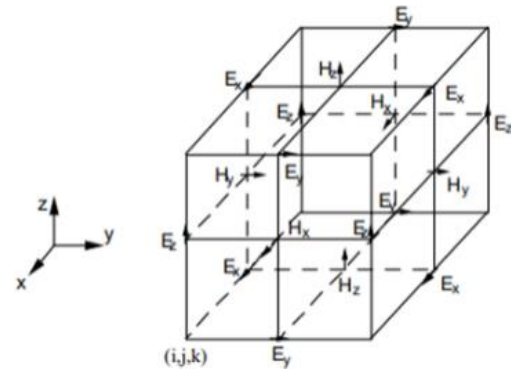

Fig. 1. Yee cell and electromagnetic fields components [38]

The mathematical formalism of Maxwell equations, which deeply describes the movement of electric and magnetic fields, is shown in Eqs. (4-6) [39]. These equations serve as fundamental principles governing the interplay between electric and magnetic phenomena in electromagnetism.

$$\partial\vec{D}/\partial t = \left(1/\sqrt{\varepsilon_0\mu_0}\right).\vec{\nabla}\times\vec{H} \tag{4}$$

$$\vec{D}(\omega) = \varepsilon_r(\omega).\vec{E}(\omega) \tag{5}$$

$$\partial\vec{H}/\partial t = \left(-1/\sqrt{\varepsilon_0\mu_0}\right).\vec{\nabla}\times\vec{E} \tag{6}$$

Where $\vec{D}$ represents electric flux density, $\vec{H}$ denotes magnetic field intensity, and $\vec{E}$ denotes the electric field. The FDTD method allows the calculation of electromagnetic fields at different frequencies and times. Maxwell equations contain important parameters like ε_r, representing relative electric permittivity, and μ_r, magnetic permeability, especially in relation to magnetic materials.

2

Therefore, to solve Maxwell equations for the solar spectrum in the simulated area of the sample, it is necessary to know $\varepsilon_r(\omega)$ or $n(\omega)$ and $k(\omega)$ [39].

In this particular study, μ_r is treated as being one. The calculation initiates with E_0, denoting the value of the electric field at $t = 0$, followed by the magnetic field (H) computation at a 0.002 fs time step. To conduct the calculation inside a specified spatial area, discretization of the computation area occurs through the subdivision into Yee cells. These samples possess a minimum size of 0.002 nm in areas characterized by rapid changes in refractive index. The refractive index in these unit cells is established in advance according to the properties of the materials. In areas of uniform materials with greater dimensions situated away from the edges, the mesh size can be enhanced to 10 nm to speed up computational efficiency. Additionally, selecting suitable boundary conditions is crucial. The Z direction uses the perfectly matched layer (PML) boundary condition, deliberately signified after the source and the lowest level. This allows the model to absorb incident light and prevents it from reradiating back into the simulation space [40]. The X and Y directions use periodic boundary conditions to complement the periodic characteristic of the nanosphere arrays [38]. Following the computation of Maxwell's formulas, the Poynting vector is determined to evaluate the absorbed optical power [41]. In the simulation phase concerning the electrical attributes of the samples, suitable voltage intervals are chosen, taking into account 300 K. The emitter layer is set to zero voltage. In contrast, the base layer is given a voltage range of 0 to 0.8 V. The current density is obtained from the calculations of the drift-diffusion and nonlinear Poisson formulas [41]. The drift-diffusion formulas explain the movement of excitons. In contrast, the nonlinear Poisson formula defines the distribution of electrostatic potential resulting from these excitons [41].

$$\vec{\nabla}.\left(\mu_n.\vec{\nabla}_n - qD_n.\vec{\nabla}p\right) + G - R = 0 \qquad (7)$$

$$\vec{\nabla}.\left(\mu_p.\vec{\nabla}_p - qD_p.\vec{\nabla}n\right) - G + R = 0 \qquad (8)$$

These equations feature electron (n) and hole (p) densities, electron (μ_n) and hole (μ_p) mobilities, and electron (D_n) and hole (D_p) diffusion coefficients. The elementary charge is denoted as q, G signifies the carrier generation rate, and R demonstrates the recombination rate. The corresponding Poisson formula is expressed as [41]:

$$\vec{\nabla}.\left(\varepsilon\overline{\nabla\Phi}\right) = -\rho/q \qquad (9)$$

Within this mathematical expression, ε stands for the relative permittivity, Φ denotes the electrostatic potential, and ρ determines the charge density. To determine the current density, the subsequent equation can be employed [41]:

$$\vec{J} = q\left(n\vec{E}\mu_n + p\vec{E}\mu_P\right) \qquad (10)$$

Within this mathematical expression, q represents the elementary charge, μ_n, and μ_p stand for the mobilities of electrons and holes. At the same time, n and p denote the carrier densities of electrons and holes, respectively. Additionally, E signifies the electric field [41].

The total power (P) can be calculated by multiplying the current density by the applied voltage (V) [41]:

$$P = J * V \qquad (11)$$

This study examines a CIGS solar cell incorporating gold, silver, and aluminum nanosphere arrays in its active layer. According to Figure 2, the p-type CIGS material acts as the absorber, converting photon energy into electrical current. At the same time, the n-type CdS buffer layer and transparent conductive oxide (TCO) layer (typically zinc oxide) serve as the window. Silver (Ag) and molybdenum are used for the front and back electrodes, respectively. The reference sample lacks nanospheres. The study compares structural characteristics of nanosphere arrays with varying size, Occupied Factor (O.F.), and positions within the absorber layer (bottom, middle, top) under broadband light (350 to 1150 nm). Optical and electrical characteristics of the samples are simulated and compared. Structural information is given in Table 1.

Table 1. The structural and electrical features of the layers [40, 42-48]

Material	Thickness			Doping type	Doping (cm⁻³)	Band gap (eV)	Work function (eV)	Permittivity (ε) (F/m)
	x-axis (nm)	y-axis (nm)	z-axis (nm)					
ZnO	500	500	80	n-type	1 e+20	3.3	-	9
CdS	500	500	60	n-type	1 e+18	2.56	-	10
CIGS	500	500	1000	p-type	1 e+16	1.2	-	13.6
Mo	500	500	500	-	-	-	4.6	-
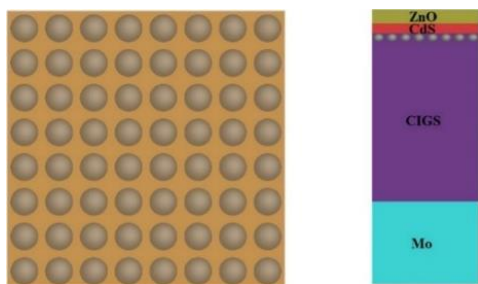
Fig. 2. Schematic layout of the simulated solar cell. On the left is the periodic arrangement of plasmonic nanospheres (top view), and on the right is the side view of the solar cell with nanospheres on top of the active layer

3. RESULTS AND DISCUSSION

3.1. Optical Results

The research evaluates the enhancement of light trapping and absorption by incorporating plasmonic nanospheres of silver (Ag), gold (Au), and aluminum (Al) into the absorber layer of CIGS solar cells. The nanospheres were systematically sized at 50 nm, 100 nm, and 200 nm in diameter, allowing for optical analysis dependent on sizes and position (i.e., top, middle, and bottom (within) the absorber layer). Additionally, to define surface coverage, the concept of occupied factor scaling nominally at 0.16 (low coverage) and 0.64 (high coverage) was employed.

The configurations of the nanospheres are based on baseline nomenclature, such that (Diameter-O.F.-Position) corresponds to L=200-O.F.=0.64-T, which represents 200 diameter nanospheres with O.F. of 0.64 in the top region of the absorber. The strategic placement of plasmonic nanostructures at the top of the absorber layer represents a critical balance between light-trapping enhancement and potential shadowing effects.

Although top-placed nano-particles theoretically take up space, and they block photons that the CIGS layer should absorb, our simulations indicate that the contribution of the plasmonic light-trapping effect vastly overcomes that of a minor shadowing loss due to the nanostructures. Though aluminum nanospheres (200 nm, O.F.= 0.64) at the top are mostly effective forward scatterers that redirect incident light at an angle into the CIGS layer, the effective optical path length within the absorbing layer is greater than that for normal incidence light and again makes up for lost direct shadowing. This phenomenon has been experimentally verified by previous research [49]. As explained

in fundamental light scattering theory, "the scattering cross-section of nanoparticles can exceed their geometric cross-section by orders of magnitude at plasmon resonance", creating a net positive effect on light absorption [34, 35]. Plasmonic nano-structures modify the refractive index of the CIGS absorber layer, whereas the reference sample assumes a constant refractive index (dependent only on the wavelength of light). The absorption curve shows clear peaks and valleys as a result of scattering and plasmonic resonances. Scattering occurs in situations where the metal nano-structures change the direction of light, either trapping it in the solar cell or reducing the amount of absorption if the light is redirected outside the solar cell. Localized surface plasmon resonances (LSPR) at specific wavelengths enhance absorption, resulting in peaks.

However, plasmonically active nanostructures that are either too large or too close together can cause parasitic losses that impact overall performance. Figure 3 addresses the effect of nanosphere diameter, nanosphere material type, and location on the CIGS active layer's absorption characteristics. The three examined metals (Ag, Au, and Al) have notably different dielectric functions that allow LSPR to be excited over a wide range of energies spanning from the visible to near infrared (NIR) regions [53]. LSPR is activated by incident photons that, in turn, excite the collective oscillation of conduction electrons at the surface of the nanoparticle, enabling enhanced scattering and near-field enhancements. The spectral location, as well as intensity, of the resonance is susceptible to the size, shape, and surrounding dielectric environment of the nanoparticles, as well as intrinsic optical properties. The diameter of plasmonic nanospheres plays a key role in determining the LSPR characteristics through mechanisms we can understand using Mie theory. For example, with increasing particle size, the additional phase difference works against the electromagnetic field acting across the particle surface, ultimately giving rise to a red-shifting of the resonance. There was a significant red shift of ~600 nm to depths of ~800-1100 nm from increasing the Al nanosphere diameter from 50 nm to 200 nm. This places the resonance at the precise location where CIGS has correspondingly weak intrinsic absorption and seeks to enhance the phenomena where it is really needed. Smaller nanoparticles (50 nm) only support dipolar resonances, which

are determined mainly by the charge distribution of the conduction electrons. In contrast, higher-order multipole modes (quadrupole, etc.) are supported by larger nanoparticles (200 nm) during dispersive excitation and produce a broader resonance profile [53]. The larger particles also have stronger scattering-to-absorption ratios, which are favorable for light-trapping applications. Scattering is the goal for light trapping in solar cells [22]. Aluminum nanoparticles of 200 nm diameter achieve an optimal balance in the NIR region. A 200 nm Al nanosphere exhibits a broad resonance spanning 800-1100 nm, overlapping with CIGS's weak absorption region near its band edge. This enables significant near-field enhancement where semiconductor absorption is low, boosting photocarrier generation in the NIR, a key factor in enhancing short-circuit current density (Jsc). In contrast, the smaller nanospheres (50 nm) will show only dipolar resonances within shorter wavelengths (< 600 nm), which will certainly be well absorbed by CIGS and therefore will not provide as good trapping of light. Silver and gold also displayed sharper resonances in the visible, because of the decreased damping, but reduced their plasmonic activity in the NIR, which has diminished their utility for thin CIGS cells, where NIR absorption is critical [49, 50]. One important factor is where the nanospheres are positioned within the absorber layer. Al nanospheres function as effective forward scatterers when placed at the top, rerouting incident light at oblique angles into the CIGS layer and lengthening the effective optical path. In order to maximize scattering cross-section and decrease near-field coupling and parasitic losses, the periodic configuration with O.F.= 0.64 guarantees enough inter-particle spacing. The plasmonic light-trapping effect more than makes up for whatever slight shadowing that top-positioned nanospheres might produce. On the other hand, nanospheres in the intermediate or lower structural layers have poorer coupling with incident light and less near-field enhancement as the electromagnetic field intensity decreases with depth. The efficiency of light-nanosphere interactions at deeper places is reduced as a result of the progressive attenuation of electromagnetic wave intensity brought on by absorption and scattering in the top layers. In contrast to the desired absorption in the active layer, parasitic absorption within the nanospheres rises under these circumstances, especially when made of metallic materials with large ohmic losses. Rather than being transformed into electron-hole pairs at the active layer, the energy of photons travelling through the top layers is primarily lost as heat inside the nanospheres, resulting in non-productive energy loss. At wavelengths that are not in line with the nanospheres' surface plasmon resonance, this increase in parasitic absorption is particularly noticeable. Nevertheless, these nanospheres function as subwavelength scatterers. These redirecting photons that have passed through the active layer, particularly at longer wavelengths, are initially prevented from being absorbed back into the active layer by lower absorption coefficients. This light-trapping effect increases the likelihood of photon reabsorption through multiple light passes and longer effective path length. We can say that the lower-positioned nanospheres produce scattering, which creates waveguide modes or indirect scattering, recycling light in the active layer, providing multiple chances for absorption. Although locally the near-field effects become less significant, at larger length scales, the global effect can offset all of the parasitic losses. Therefore, this increases the net optical absorption efficiency of the structure. Thus, the optimal configuration of Al nanospheres (200 nm, O.F.= 0.64) at the top maximizes both scattering efficiency and near-field enhancement in the most absorption-deficient spectral region. The aluminum nanospheres (200 nm, O.F.= 0.64) exhibit strong forward scattering and localized field enhancement due to LSPR, boosting absorption in the underlying CIGS layer. This plasmonic light-trapping effect compensates for and surpasses any minor shadowing loss, resulting in a net increase in photocurrent and efficiency. According to Table 2, plasmonic components in CIGS solar cells boost light absorption, which results in a markedly larger creation of electron-hole pairs—up to 10^3 times higher than in bare cells. This improvement results from a strong interaction between surface plasmon resonances (SPPs and LSPRs) and incident light, which increases exciton formation and strengthens the local electromagnetic field. Furthermore, plasmon resonance creates high-energy hot electrons that are injected into the active layer and improve carrier generation by ionization by transferring photon energy to conduction electrons [51]. However, great overall efficiency

Marzieh Akbari et al.

is not guaranteed by effective charge carrier generation alone. Recombination, transport, and charge extraction are also important processes. Performance can be decreased by poorly designed nanostructures that increase recombination or parasitic losses (like heat). Plasmonic design optimization is therefore crucial for optimizing electrical output as well as absorption. According to Table 2, silver nano-spheres with diameters of 100–200 nm and O.F.= 0.16–0.64 that are positioned at the bottom of the absorber produce the most excitons (10^3 times that of the bare cell). The need to investigate the electrical effects of plasmonic integration is highlighted by the fact that, even if these plasmonic structures improve charge creation through enhanced absorption and localized electric fields close to electrodes, effective extraction and

transport of these carriers are still crucial [52]. The difference between plasmon decay channels that are radiative (scattering) and non-radiative (absorption) is important, and aluminum's wider resonance is beneficial for NIR enhancement in CIGS. Furthermore, plasmonic structures can both increase carrier generation and possibly add recombination centers; aluminum performs better in this balancing than noble metals because of its advantageous band alignment and lower interfacial recombination [24, 25].

3.2. Electrical Results

The combination of plasmonic nanostructures substantially affects the electrical performance of CIGS solar cells, as reflected in the I–V and P–V characteristics (Figs. 4 and 5).
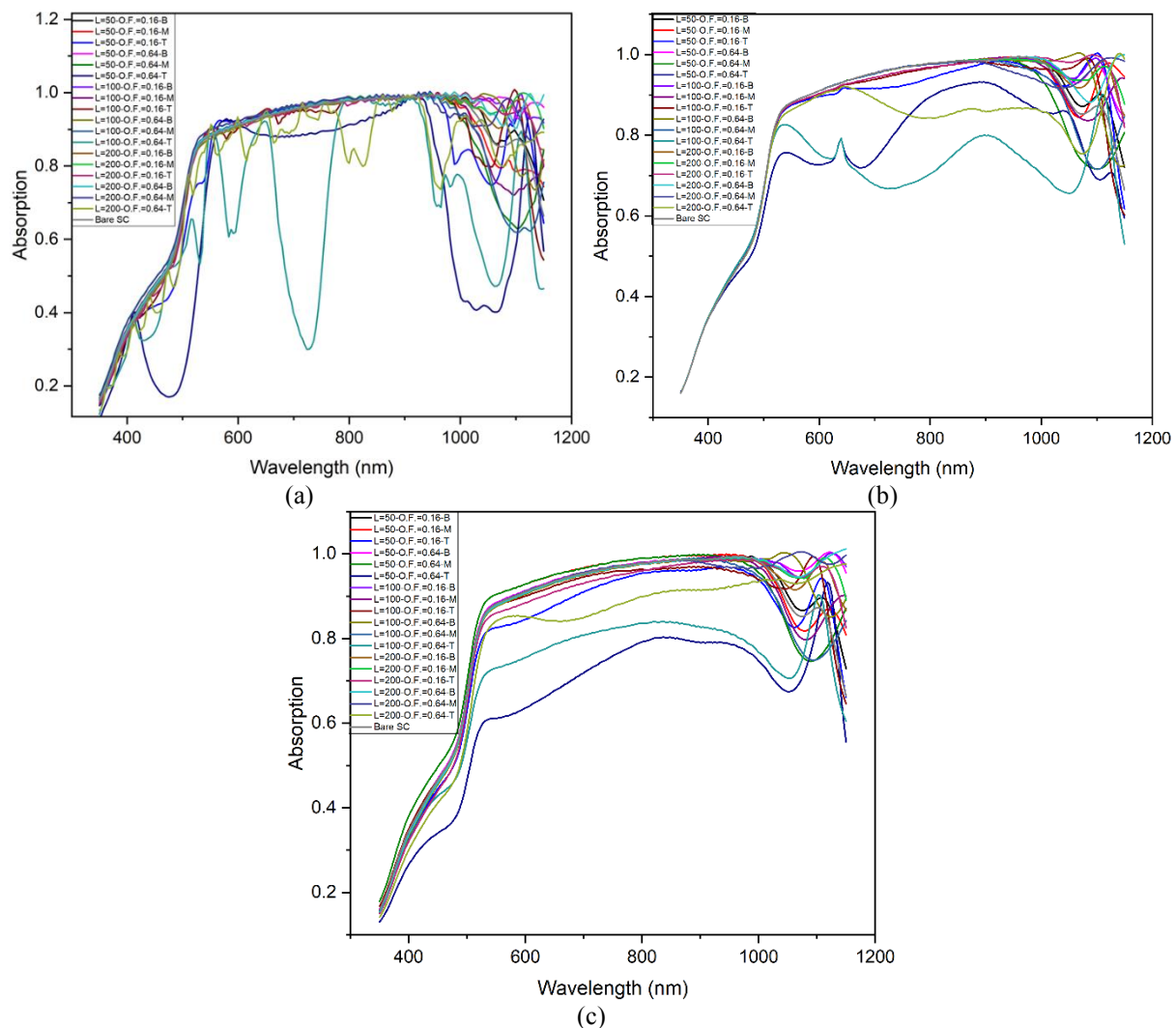
Fig. 3. Absorption diagram by wavelength in the cell with a) silver, b) gold, c) aluminium nanospheres for various diameters, occupied factor of nanospheres on the bottom (B), middle (M) and top (T) of the absorbent layer

[Downloaded from pga.iust.ac.ir on 2026-02-15]

[DOI: 10.22068/ijmse.4000]

6

Table 2. Data of the Generation rate of electron-hole pairs for samples by silver, gold, and aluminium nanostructures at different diameters, occupied factor, and locations of plasmonic nanostructures

Size	O.F= 0.16			O.F= 0.64		
	Bottom	Middle	Top	Bottom	Middle	Top
Al						
50	1.64E+28	1.72E+28	1.35E+29	2.35E+28	2.82E+28	1.32E+29
100	6.28E+28	2.37E+28	9.35E+28	2.15E+28	1.63E+28	9.74E+28
200	1.44E+29	3.09E+28	7.43E+28	2.15E+28	3.21E+28	8.51E+28
Au						
50	1.65E+28	1.91E+28	7.49E+28	1.64E+28	1.65E+28	6.15E+28
100	2.23E+28	5.53E+28	7.39E+28	1.64E+28	2.14E+28	8.52E+28
200	4.96E+28	1.77E+28	6.90E+28	2.92E+28	3.83E+28	5.39E+28
Ag						
50	2.44E+29	6.38E+28	1.56E+29	3.60E+29	3.52E+28	1.24E+29
100	7.46E+30	1.14E+29	4.49E+29	5.86E+29	8.71E+28	1.30E+29
200	4.08E+30	1.31E+29	2.98E+29	2.00E+30	1.94E+29	1.96E+29

Plasmonic structures improve the I–V response, as well as the generated and extracted carriers, when we compare Figs. 4 and 5 with the bare cell. The improvement is derived not only from scattering but also from resonant near-field enhancements and stronger local fields, which favor exciton dissociation and limit radiative recombination [16]. As such, the number of free carriers collected at the electrodes increases, generating a more even carrier generation profile, and through the enhanced generation, reducing space-charge buildup that improves transport. The observed improvement in J_{sc} for the Al-L=200-O.F.=0.64-T sample (36.80 mA/cm²) is purely related to plasmon-generated absorption in the NIR (Table 2). While silver nanostructures present some of the highest generation rates (as an example: Ag-L=200-O.F.=0.16-B: 4.08×10^{30} cm^{-3}s^{-1}), their parasitic absorption and poor charge extraction-particularly at the junction-drastically affect their electrical performance. This discrepancy is attributed to conductive pathways, or recombination centers, that deteriorate fill factor and Voc. Although aluminum has greater intrinsic losses, it benefits from good band alignment and lower interfacial recombination, protecting device quality. The P-V curves (Fig. 5) show the relationship between output power and applied voltage, with the maximum power point (MPP) showcasing the best condition. Output power is current multiplied by voltage, so any loss in current will cause an immediate loss in power, demonstrating the importance of maximizing the J_{sc} and V_{oc} simultaneously [54]. The open-circuit voltage is a result of bandgap, doping, and the shape of the

nanosphere. At the same time, the short-circuit current is based on absorbing light, generating carriers and the efficiency of extraction. The fill factor (FF) is another characterization for cell quality, as it is defined as the MPP divided by J_{sc} multiplied by V_{oc}. Optimized plasmonic structures increase all three parameters. The Al-L=200-O.F.=0.64-T sample achieved the highest V_{oc} (0.8745 V), J_{sc} (36.80 mA/cm²), and overall efficiency (26.14%). A silver nanosphere sample (100 nm, O.F.= 0.64, top) recorded the highest FF (0.8285), but suffered from recombination, limiting its efficiency [55]. The performance of the materials shows the comparisons made were different: Ag (100 nm, O.F.= 0.16, top) was 23.92% efficient, Au (100 nm, O.F.= 0.16, top) was 25.29% efficient, and Al (200 nm, O.F.= 0.64, top) was the highest performer with an efficiency of 26.14%. It should be noted that other studies have shown similar improvement with Au nanocubes (100 nm, O.F.= 0.16) with a maximum efficiency of 25.61% [56]. Furthermore, aluminum was the best-performing material, it is also the least expensive compared to Ag and Au for large-scale applications. Although the absorption was slightly less than a bare cell, the Al-based structures generated 10 times the charge carriers due to enhanced near-field intensities, improved carrier collection, and minimal effects to transport charges to the external circuit. The simulated efficiency of our bare cell of 19.3%. This approach is very similar to the similar cell that Ramanathan et al. stated had an efficiency of 19% in 2005, which is an approximate relative error of 1.6%. Since the two efficiencies are close to one

another, these results support the validity of our simulation results [57].The purpose of this study must also be contextualized among similarly recent progress in plasmonic solar cells. In direct comparison to the MIM waveguide by Ping (2024), which notes a 55% increase in solar cell performance at a 65° angle of incidence, our design presents an impressive 7.11% absolute efficiency increase (26.14%) at normal incidence (AM1.5G), utilizing a much simpler and thus much more practical design based on Al nanospheres [58]. The MIM structure is a sophisticated, multi-layered structure, and although it is functioning effectively, it poses manufacturing issues for large-scale CIGS production. On the other hand, the Al nanospheres mounted on top in this work are low-cost and CMOS compatible, while being highly adaptable to industrial applications. Additionally, while Waketola et al. (2025) have showcased Ag and Au nanoparticles for plasmonic organic solar cells, our findings have shown that aluminum performs better with CIGS-based devices, especially in the near-infrared (NIR) region (800–1100 nm), where CIGS is insufficiently able to absorb extrinsically [59]. However, the Al nanospheres exhibited broad plasmonic resonance (200 nm, O.F.= 0.64), which could mitigate the limitation mentioned above and encourage carrier generation without the use of noble metals and for much lower fabrication costs. Contrasting with Hasheminassab et al. (2021), who propose applying Ag nanoparticles to CIGS cells, we provide not only optical absorption but a thorough opto-electrical analysis (J_{sc}, V_{oc}, FF, and recombination) [60].
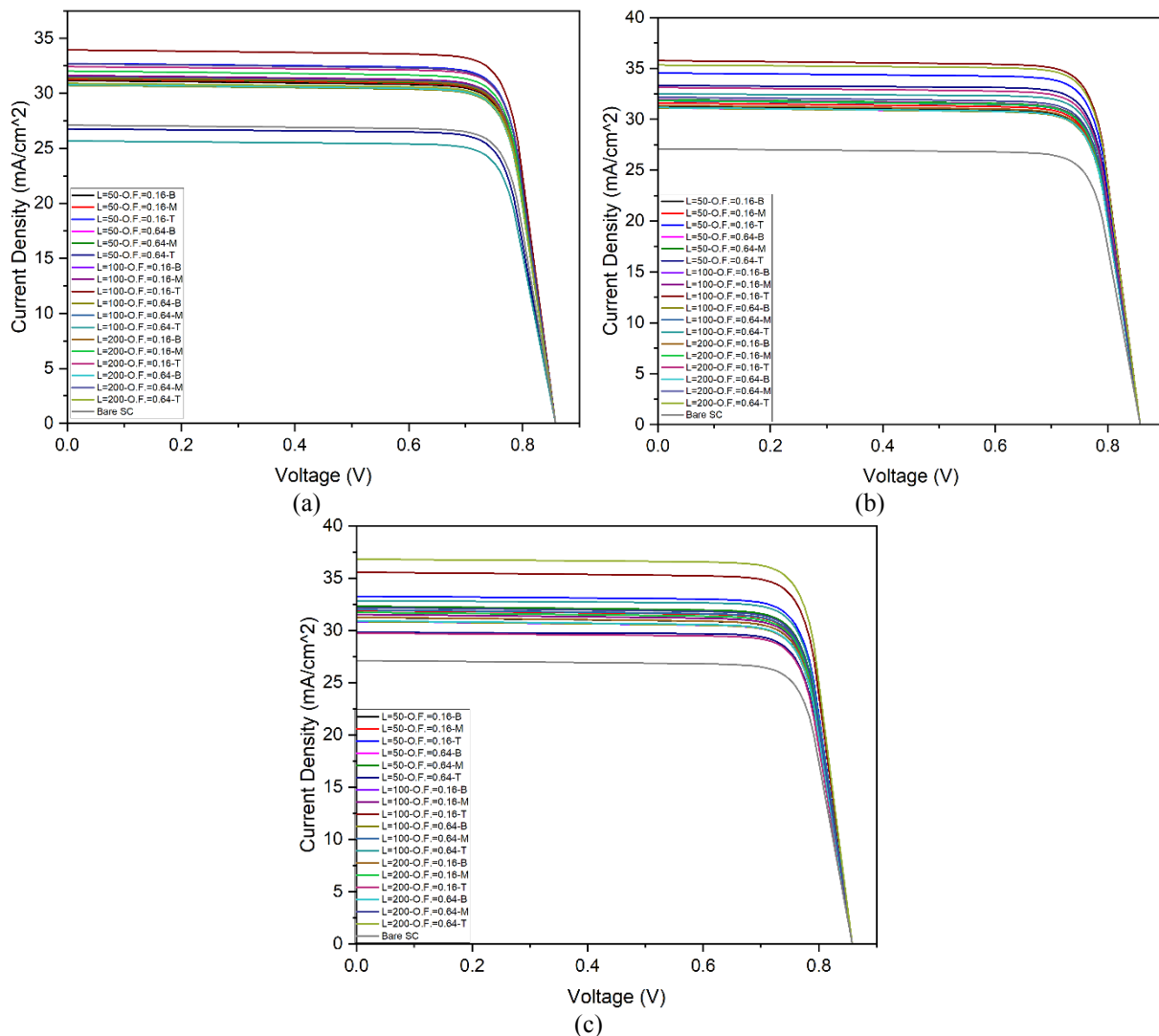
Fig. 4. Current-voltage diagram in the cell with a) silver, b) gold, c) aluminium nanospheres for various diameters, occupied factor of nanospheres on the bottom (B), middle (M), and top (T) of the absorbent layer
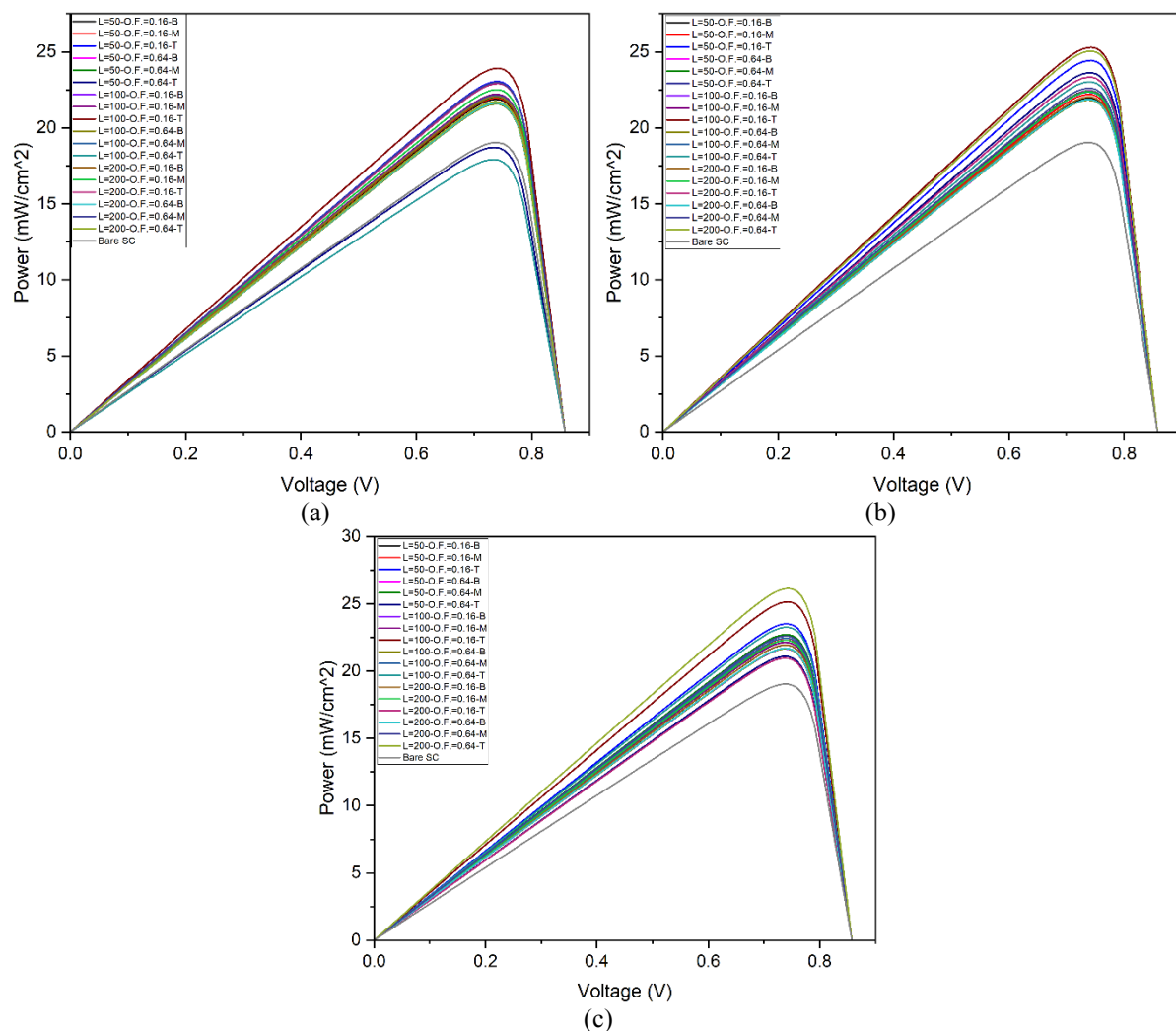
Fig. 5. Diagram of power-voltage of solar cell in the cell with a) silver, b) gold, c) aluminium nanospheres for various diameters, occupied factor of nanospheres on the bottom (B), middle (M), and top (T) of the absorbent layer

Table 3. Data of Efficiency for samples by silver, gold, and aluminium nanospheres at different diameters, occupied factor, and locations of nanospheres

Size	O.F=0.16			O.F=0.64		
Al						
50	21.93%	22.42%	23.50%	21.69%	22.71%	21.09%
100	21.65%	22.14%	25.15%	21.66%	22.45%	23.25%
200	21.94%	22.28%	20.95%	21.70%	22.60%	26.14%
Au						
50	21.95%	22.20%	24.43%	21.84%	22.44%	23.63%
100	21.85%	22.41%	25.29%	21.84%	22.35%	23.03%
200	22.03%	22.38%	23.33%	21.87%	22.61%	25.05%
Ag						
50	21.88%	21.96%	23.05%	21.57%	22.02%	18.72%
100	21.65%	22.21%	23.92%	21.56%	22.12%	17.92%
200	22.06%	22.51%	22.06%	21.62%	22.99%	21.72%

We can also deduce that a forward scattering optimisation and the lack of parasitic losses can be achieved by placing plasmonic nanostructures on top of the absorber, rather than on the bottom

or interior of the cell, which requires parasitic losses to generate electrical output. Such findings are encouraged by researchers such as Chen et al. (2014), who demonstrated experimental confirmation of efficiency improvement by placing Au nanoparticles onto the CIGS surface (where the efficiency improved from 8.31% to 10.36%), with enhancements being significantly noted in J_{sc} and FF [61]. The strong correlation between our simulations and the published data from Chen and colleagues validates the mechanisms we have presented. It supports that plasmonic structures are capable of enhancing carrier generation and collection. Overall, our detailed investigation establishes that aluminum nanospheres are an inexpensive, scalable, and practical route for next-generation CIGS photovoltaics.

4. CONCLUSIONS

CIGS solar cells are receiving high consideration because of the low cost of production and high efficiency values, as they outperform normal silicon cells under the same conditions. This paper presents the contribution of plasmonic nanospheres through a thorough analysis of how to measure their efficiency in a CIGS cell, by enhancing light absorption, exciton generation, and reducing recombination. We have analysed the various sizes, arrangements, and placements of plasmonic nanospheres using opto-electrical simulations, which utilised absorption curves, exciton generation, and electrical parameters (J_{sc}, V_{oc}, fill factor, and efficiency). The highest efficiency (26.14%) came from utilizing 200 nm aluminium nanospheres (O.F.= 0.64) placed at the very top of the absorber layer, an improvement of 7.11% efficiency from the bare cell, demonstrating the possibilities of CIGS while maintaining it can and should be designed with thorough investigation and implementation of all losses during a complete cycle of generated carriers from exciton creation to carrier generation, output, and recombination losses.

ACKNOWLEDGMENTS

REFERENCES

[1] Moon SH, Park SJ, Kim SH, Lee MW, Han J, Kim JY, Kim H, Hwang YJ, Lee DK, Min BK. "Monolithic DSSC/CIGS tandem solar cell fabricated by a solution process". Sci. Rep. 2015, 5, 8970.

[2] Li X, Ma B, Wang C, Hu D, Lü Y, Chen Y. "Recycling and recovery of spent copper—indium—gallium—diselenide (CIGS) solar cells: A review". Int. J. Miner., Metall. Mater. 2023, 989-1002.

[3] Mufti N, Amrillah T, Taufiq A, Diantoro M, Nur H. "Review of CIGS-based solar cells manufacturing by structural engineering". Solar energy. 2020, 207, 1146-57.

[4] Wang YC, Wu TT, Chueh YL. "A critical review on flexible Cu (In, Ga) Se2 (CIGS) solar cells". Mater. Chem. Phys. 2019, 234, 329-44.

[5] Saparov B. "Next generation thin-film solar absorbers based on chalcogenides". Chem. Rev. 2022, 122, 10575-7.

[6] Bhatt V, Kim ST, Kumar M, Jeong HJ, Kim J, Jang JH, Yun JH. "Impact of Na diffusion on Cu (In, Ga) Se2 solar cells: Unveiling the role of active defects using thermal admittance spectroscopy". Thin Solid Films. 2023, 767, 139673.

[7] Nakamura M, Yamaguchi K, Kimoto Y, Yasaki Y, Kato T, Sugimoto H. "Cd-free Cu (In, Ga)(Se, S) 2 thin-film solar cell with record efficiency of 23.35%". IEEE J Photovolt. 2019, 9, 1863-7.

[8] Chang Q, Yuan S, Fu J, Gao Q, Zhao Y, Xu Z, Kou D, Zhou Z, Zhou W, Wu S. "Interface engineering for high-efficiency solution-processed Cu (in, Ga)(S, Se) 2 solar cells via a novel indium-doped CdS strategy". ACS Appl Mater Interfaces. 2022, 14, 5149-58.

[9] Czudek A, Urbaniak A, Eslam A, Wuerz R, Igalson M. "Potassium versus sodium in Cu (In, Ga) Se2—similarities and differences in the electrical characteristics of solar cells and thin films after NaF or KF postdeposition treatment". Phys Status Solidi Rapid Res Lett. 2022, 16, 2100459.

[10] Heriche H, Rouabah Z, Bouarissa N. "High-efficiency CIGS solar cells with optimization of layers thickness and doping". Optik. 2016, 127, 11751-7.

[11] Mina MS, Kim S, Enkhbat T, Enkhbayar E, Kim J. "High Efficiency Aqueous Solution Sprayed CIGSSe Solar Cells: Effects of

Zr4+-Alloyed In2S3 Buffer and K-Alloyed CIGSSe Absorber". Adv. Funct. Mater. 2022, 32, 2206561.

[12] Yang SC, Lin TY, Ochoa M, Lai H, Kothandaraman R, Fu F, Tiwari AN, Carron R. "Efficiency boost of bifacial Cu (In, Ga) Se2 thin-film solar cells for flexible and tandem applications with silver-assisted low-temperature process". Nature Energy. 2023, 8, 40-51.

[13] Shockley W, Queisser H. Detailed balance limit of efficiency of p–n junction solar cells. InRenewable energy, 2018, pp. Vol2_35-Vol2_54.

[14] Royanian S, Abdolahzadeh Ziabari A, Yousefi R. "Efficiency enhancement of ultra-thin CIGS solar cells using bandgap grading and embedding Au plasmonic nanoparticles". Plasmonics. 2020, 15, 1173-82.

[15] Day J, Senthilarasu S, Mallick TK. "Improving spectral modification for applications in solar cells: A review". Renewable Energy. 2019, 132, 186-205.

[16] Gharibshahian I, Sharbati S, Orouji AA. "Potential efficiency improvement of Cu (In, Ga) Se2 thin-film solar cells by the window layer optimization". Thin Solid Films. 2018, 655, 95-104.

[17] Ghamsari-Yazdel F, Gharibshahian I, Sharbati S. "Thin oxide buffer layers for avoiding leaks in CIGS solar cells; a theoretical analysis". J. Mater. Sci.: Mater. Electron. 2021, 32, 7598-608.

[18] Gharibshahian I, Orouji AA, Sharbati S. "Effectiveness of band discontinuities between CIGS absorber and copper-based hole transport layer in limiting recombination at the back contact". Mater. Today Commun. 2022, 33, 104220.

[19] Ahmadpanah FS, Orouji AA, Gharibshahian I. "Improving the efficiency of CIGS solar cells using an optimized p-type CZTSSe electron reflector layer". J. Mater. Sci.: Mater. Electron. 2021, 32, 22535-47.

[20] Sharbati S, Gharibshahian I, Orouji AA. "Designing of $Al_xGa_{1-x}As$/CIGS tandem solar cell by analytical model". Solar Energy. 2019, 188, 1-9.

[21] Sharbati S, Gharibshahian I, Orouji AA. "Proposed suitable electron reflector layer materials for thin-film $CuIn_{1-x}Ga_xSe_2$ solar cells". Optical Materials. 2018, 75, 216-23.

[22] Atwater HA, Polman A. "Plasmonics for improved photovoltaic devices". Nat. Mater. 2010, 9, 205-13.

[23] Oliveira AJ, Teixeira JP, Ramos D, Fernandes PA, Salomé PM. "Exploiting the optical limits of thin-film solar cells: a review on light management strategies in Cu (In, Ga) Se2". Adv. Photonics Res. 2022, 3, 2100190.

[24] Zarerasouli P, Bahador H, Heidarzadeh H. "Design of an efficient ultra-thin film Cu (In, Ga) Se2 solar cell, using plasmonic cluster back reflectors". Solar Energy. 2023, 261, 1-6.

[25] Abdolahzadeh Ziabari A, Royanian S, Yousefi R, Ghoreishi S. "Performance improvement of ultrathin CIGS solar cells using Al plasmonic nanoparticles: The effect of the position of nanoparticles". JOPN. 2020 Nov 1; 5(4):17-32.

[26] Mohsin AS, Mobashera M, Malik A, Rubaiat M, Islam M. "Light trapping in thin-film solar cell to enhance the absorption efficiency using FDTD simulation". Journal of Optics. 2020, 49, 523-32.

[27] Morawiec S, Mendes MJ, Priolo F, Crupi I. "Plasmonic nanostructures for light trapping in thin-film solar cells". Mater. Sci. Semicond. Process. 2019, 92, 10-8.

[28] Tabrizi AA, Pahlavan A. "Efficiency improvement of a silicon-based thin-film solar cell using plasmonic silver nanoparticles and an antireflective layer". Opt. Commun. 2020, 454, 124437.

[29] Peter Amalathas A, Alkaisi MM. "Nanostructures for light trapping in thin film solar cells". Micromachines. 2019, 10, 619.

[30] Gobinath Velu, Fundamentals of Solar Cell Design, John Wiley & Sons, Hoboken, USA, 2021.

[31] Erwin WR, Zarick HF, Talbert EM, Bardhan R. "Light trapping in mesoporous solar cells with plasmonic nanostructures". Energy Environ. Sci. 2016, 9, 1577-601.

[32] AlZoubi T, Moustafa M. "Numerical optimization of absorber and CdS buffer layers in CIGS solar cells using SCAPS". Int. J. Smart Grid Clean Energy. 2019, 8, 291-8.

[33] Massiot I, Cattoni A, Collin S. "Progress and prospects for ultrathin solar cells".

11

Nature Energy. 2020, 5, 959-72.

[34] Li H, Hu Y, Yang Y, Zhu Y. "Theoretical investigation of broadband absorption enhancement in a-Si thin-film solar cell with nanoparticles". Sol. Energy Mater. Sol. Cells. 2020, 211, 110529.

[35] Mandal P. "Application of plasmonics in solar cell efficiency improvement: a brief review on recent progress". Plasmonics. 2022, 17, 1247-67.

[36] Yang WJ, Ma ZQ, Tang X, Feng CB, Zhao WG, Shi PP. "Internal quantum efficiency for solar cells". Solar Energy. 2008, 82, 106-10.

[37] Karki S, Paul P, Rajan G, Belfore B, Poudel D, Rockett A, Danilov E, Castellano F, Arehart A, Marsillac S. "Analysis of recombination mechanisms in RbF-treated CIGS solar cells". IEEE J Photovolt. 2018, 9, 313-8.

[38] Moliton A, Nunzi JM. "How to model the behaviour of organic photovoltaic cells". Polym. Int. 2006, 55, 583-600.

[39] Taflove A, Hagness SC, Piket-May M. Computational electromagnetics: the finite-difference time-domain method. The Electrical Engineering Handbook. Elsevier, London, UK, 2005, 629-670.

[40] J.D. Jackson, Classical Electrodynamics, 3rd Edition. John Wiley & Sons, 1998.

[41] S. M. Sze, Physics of Semiconductor Devices, 3rd Edition. John Wiley & Sons, 2006.

[42] Benmir A, Aida MS. "Analytical modeling and simulation of CIGS solar cells". Energy procedia. 2013, 36, 618-27.

[43] Repins I, Glynn S, Duenow J, Coutts TJ, Metzger WK, Contreras MA. "Required material properties for high-efficiency CIGS modules". In Thin Film Solar Technology. 2009, 7409, 156-169.

[44] Moustafa M, Al Zoubi T, Yasin S. "Optoelectronics Simulation of CIGS-Based Solar Cells Using a Cd-Free Nontoxic ZrS_xSe_{2-x} as a Novel Buffer Layer". Braz. J. Phys. 2022, 52, 141.

[45] Paul S, Grover S, Repins IL, Keyes BM, Contreras MA, Ramanathan K, Noufi R, Zhao Z, Liao F, Li JV. "Analysis of back-contact interface recombination in thin-film solar cells". IEEE J Photovolt. 2018, 8, 871-8.

[46] Taretto K, Rau U. "Numerical simulation of carrier collection and recombination at grain boundaries in Cu (In, Ga) Se2 solar cells". J. Appl. Phys. 2008, 103.

[47] Cho KS, Jang J, Park JH, Lee DK, Song S, Kim K, Eo YJ, Yun JH, Gwak J, Chung CH. "Optimal CdS buffer thickness to form high-quality CdS/Cu (In, Ga) Se2 junctions in solar cells without plasma damage and shunt paths". ACS omega. 2020, 5, 23983-8.

[48] Kamikawa Y, Nishinaga J, Shibata H, Ishizuka S. "Efficient narrow band gap Cu (In, Ga) Se2 solar cells with flat surface". ACS Appl. Mater. Interfaces. 2020, 12, 45485-92.

[49] Hasheminassab SM, Imanieh M, Kamali A, Emamghorashi SA, Hassanhosseini S. "Influence of the shape and size of Ag nanoparticles on the performance enhancement of CIGS solar cells: the role of surface plasmons". Plasmonics. 2021, 16, 273-82.

[50] Dal Forno S, Ranno L, Lischner J. "Material, size, and environment dependence of plasmon-induced hot carriers in metallic nanoparticles". J. Phys. Chem. C. 2018, 122, 8517-27.

[51] Zhan C, Chen XJ, Yi J, Li JF, Wu DY, Tian ZQ. "From plasmon-enhanced molecular spectroscopy to plasmon-mediated chemical reactions". Nat. Rev. Chem. 2018, 2, 216-30.

[52] Tang H, Chen CJ, Huang Z, Bright J, Meng G, Liu RS, Wu N. "Plasmonic hot electrons for sensing, photodetection, and solar energy applications: A perspective". J. Chem. Phys. 2020, 152.

[53] Cheng YW, Xue HT, Tang FL, Liu JL. First-Principles Simulations for CuInGaSe2 (CIGS) Solar Cells. InNanostructured Materials for Next-Generation Energy Storage and Conversion: Photovoltaic and Solar Energy. Springer Berlin Heidelberg, Berlin, Germany, 2019, 45-74.

[54] Boukortt NE, Patanè S, Adouane M. "Modeling and investigation of rear-passivated ultrathin CIGS solar cell". Electronics. 2023, 12, 758.

[55] Tobbeche S, Kalache S, Elbar M, Kateb MN, Serdouk MR. "Improvement of the CIGS solar cell performance: structure based on a ZnS buffer layer". Opt. Quantum Electron. 2019, 51, 284.

[56] Akbari M, Kashani FD, Mirkazemi SM. "Designing novel plasmonic architectures for highly efficient CIGS solar cells". Solar Energy. 2024, 274, 112589.

[57] Ramanathan K, Keane J, Noufi R. "Properties of high-efficiency CIGS thin-film solar cells". InConference Record of the Thirty-first IEEE Photovoltaic Specialists Conference, 2005, 195-198. IEEE.

[58] Ping S. "Design of plasmonic nanoparticles for increasing efficiency and absorptance in thin-film solar cells". Journal of Optics. 2024, 53, 404-15.

[59] Waketola AG, Tegegne NA, Hone FG. "Recent Progress in Silver and Gold Nanoparticle-Based Plasmonic Organic Solar Cells". Plasmonics. 2025, 20, 5521-56.

[60] Hasheminassab SM, Imanieh M, Kamali A, Emamghorashi SA, Hassanhosseini S. "Influence of the shape and size of Ag nanoparticles on the performance enhancement of CIGS solar cells: the role of surface plasmons". Plasmonics. 2021, 16, 273-82.

[61] Chen SC, Chen YJ, Chen WT, Yen YT, Kao TS, Chuang TY, Liao YK, Wu KH, Yabushita A, Hsieh TP, Charlton MD. "Toward omnidirectional light absorption by plasmonic effect for high-efficiency flexible nonvacuum Cu (In, Ga) Se2 thin film solar cells". ACS nano. 2014, 8, 9341-8.